

# DINO-WM: WORLD MODELS ON PRE-TRAINED VISUAL FEATURES ENABLE ZERO-SHOT PLANNING

**Gaoyue Zhou<sup>1\*</sup>, Hengkai Pan<sup>1</sup>, Yann LeCun<sup>1,2</sup>, Lerrel Pinto<sup>1</sup>**

<sup>1</sup>Courant Institute, New York University, <sup>2</sup>Meta-FAIR

## ABSTRACT

The ability to predict future outcomes given control actions is fundamental for physical reasoning. However, such predictive models, often called world models, have proven challenging to learn and are typically developed for task-specific solutions with online policy learning. We argue that the true potential of world models lies in their ability to reason and plan across diverse problems using only passive data. Concretely, we require world models to have the following three properties: 1) be trainable on offline, pre-collected trajectories, 2) support test-time behavior optimization, and 3) facilitate task-agnostic reasoning. To realize this, we present DINO World Model (DINO-WM), a new method to model visual dynamics without reconstructing the visual world. DINO-WM leverages spatial patch features pre-trained with DINOv2, enabling it to learn from offline behavioral trajectories by predicting future patch features. This design allows DINO-WM to achieve observational goals through action sequence optimization, facilitating task-agnostic behavior planning by treating desired goal patch features as prediction targets. We evaluate DINO-WM across various domains, including maze navigation, tabletop pushing, and particle manipulation. Our experiments demonstrate that DINO-WM can generate zero-shot behavioral solutions at test time without relying on expert demonstrations, reward modeling, or pre-learned inverse models. Notably, DINO-WM exhibits strong generalization capabilities compared to prior state-of-the-art work, adapting to diverse task families such as arbitrarily configured mazes, push manipulation with varied object shapes, and multi-particle scenarios.

## 1 INTRODUCTION

Robotics and embodied AI has seen tremendous progress in recent years. Advances in imitation learning and reinforcement learning has enabled agents to learn complex behaviors across diverse tasks Lee et al. (2024); Zhao et al. (2023); Ma et al. (2024); Hafner et al. (2024); Hansen et al. (2024); Agarwal et al. (2022); Haldar et al. (2024). Despite this progress, generalization remains a major challenge Zhou et al. (2023). Existing approaches predominantly rely on policies that, once trained, operate in a feed-forward manner during deployment—mapping observations to actions without any further optimization or reasoning. Under this framework, successful generalization inherently requires agents to possess solutions to all possible tasks and scenarios once training is complete, which is only possible if the agent has seen similar scenarios during training Brohan et al. (2023b;a); Reed et al. (2022); Etukuru et al. (2024). However, it is neither feasible nor efficient to learn solutions for all potential tasks and environments in advance.

Instead of learning the solutions to all possible tasks during training, an alternate is to fit a dynamics model on training data and optimize task-specific behavior during runtime. These dynamics models, also called world models Ha & Schmidhuber (2018), have a long history in robotics and control Sutton (1991); Todorov & Li (2005); Williams et al. (2017). More recently, several works have shown that world models can be trained on raw observational data Hafner et al. (2019; 2024); Micheli et al. (2023); Robine et al. (2023); Hansen et al. (2024). This enables flexible use of model-based optimization to obtain policies as it circumvents the need for explicit state-estimation. Despite this, significant challenges still remain in its use for solving general-purpose tasks.

---

\*Corresponding author. gzz123@nyu.edu

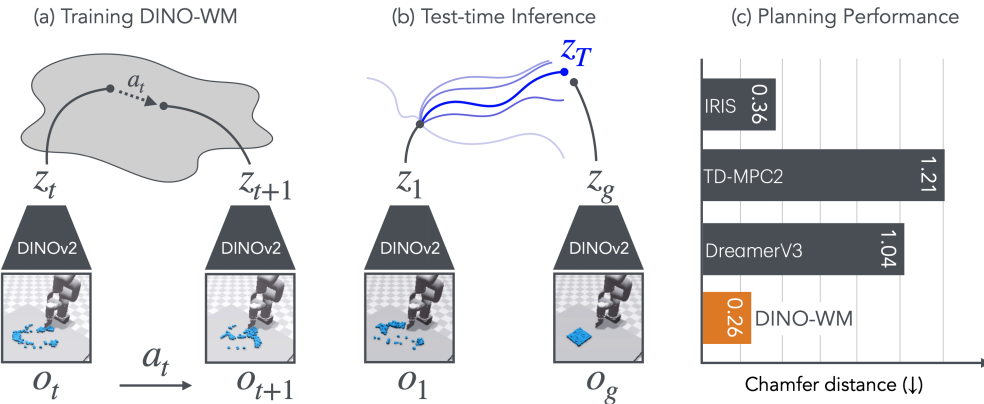


Figure 1: We present DINO-WM, a method for training visual models by using pretrained DINOv2 embeddings of image frames (a). Once trained, given a target observation  $o_T$ , we can directly optimize agent behavior by planning through DINO-WM using model-predictive control (b). The use of pretrained embeddings significantly improves performance over prior state-of-the-art world models (c).

To understand the challenges in world modeling, let us consider the two broad paradigms in learning world models: online and offline. In the online setting, access to the environment is often required so data can be continuously collected to improve the world model, which in turn improves the policy and the subsequent data collection. However, the online world model is only accurate in the cover of the policy that was being optimized. Hence, while it can be used to train powerful task-specific policies , it requires retraining for every new task even in the same environment . Instead in the offline setting, the world model is trained on an offline dataset of collected trajectories in the environment, which removes its dependence on the task specificity given sufficient coverage in the dataset. However, when required to solve a task, methods in this domain require strong auxiliary information to overcome the lack of dense coverage on the task-specific domain. This auxiliary information can take the form of expert demonstrations Pathak et al. (2018), structured keypoints Ko et al. (2023); Wen et al. (2024), access to pretrained inverse models Du et al. (2023); Ko et al. (2023) or dense reward functions , all of which reduce the generality of using offline world models. The central question to building better offline world models is if there is alternate auxiliary information that does not compromise its generality?

In this work, we present DINO-WM, a new and simple method to build task-agnostic world models from an offline dataset of trajectories. DINO-WM models the dynamics of world on compact embeddings of the world, rather than the raw observations themselves. For the embedding, we use pretrained patch-features from the DINOv2 model, which provides both a spatial and object-centric representation prior. We conjecture that this pretrained representation enables robust and consistent world modeling, which relaxes the necessity for task-specific data coverage. Given these visual embeddings and actions, DINO-WM uses the ViT architecture to predict future embeddings. Once this model is trained, planning to solve tasks is constructed as visual goal reaching, i.e. to reach a future desired goal given the current observation. Since the predictions by DINO-WM are high quality (see Figure 4), we can simply use model-predictive control with inference-time optimization to reach desired goals without any extra information during testing.

DINO-WM is experimentally evaluated on four environment suites spanning maze navigation, sliding manipulation, and particle manipulation tasks. Our experiments reveal the following findings:

- DINO-WM produce high-quality future world modeling that can be measured by improved visual reconstruction from trained decoders. On LPIPS metrics for our hardest tasks, this improves upon prior state-of-the-art work by 56% (See Section 4.7).
- Given the latent world models trained using DINO-WM, we show high success for reaching arbitrary goals on our hardest tasks, improving upon prior work by 45% on average (See Section 4.3).
- DINO-WM can be trained across environment variations within a task family (e.g. different maze layouts for navigation or different object shapes for manipulation) and achieve higher rates of success compared to prior work (See Section 4.5).

---

Code and models for DINO-WM will be open-sourced to ensure reproducibility and videos of policies are made available on our project website: <https://dino-wm.github.io>.

## 2 RELATED WORK

We build on top of several works in building world models, optimizing them, and using compact visual representations. For conciseness, we only discuss the ones most relevant to DINO-WM.

**Model-based Learning:** Learning from models of dynamics has a rich literature spanning the fields of control, planning, and robotics Sutton (1991); Todorov & Li (2005); Astolfi et al. (2008); Holkar & Waghmare (2010); Williams et al. (2017). Recent works have shown that modeling dynamics and predicting future states can significantly enhance vision-based learning for embodied agents across various applications, including online reinforcement learning Hafner et al. (2024); Micheli et al. (2023); Hansen et al. (2024); Robine et al. (2023), exploration Mendonca et al. (2021; 2023a); Sekar et al. (2020), planning Finn & Levine (2017); Ebert et al. (2018); Hafner et al. (2019), and imitation learning Pathak et al. (2018). Several of these approaches initially focused on state-space dynamics Deisenroth & Rasmussen (2011); Chua et al. (2018); Lenz et al. (2015); Nagabandi et al. (2019), and has since been extended to handle image-based inputs, which we address in this work. These world models can predict future states in either pixel space Finn & Levine (2017); Ebert et al. (2018); Ko et al. (2023); Du et al. (2023) or latent representation space Yan et al. (2021). Predicting in pixel space, however, is computationally expensive due to the need for image reconstruction and the overhead of using diffusion models . On the other hand, latent-space prediction is typically tied to objectives of reconstructing images Hafner et al. (2019; 2024); Micheli et al. (2023), which raises concerns about whether the learned features contain sufficient information about the task. Moreover, many of these models incorporate reward prediction Hafner et al. (2024); Micheli et al. (2023); Robine et al. (2023), or use reward prediction as auxiliary objective to learn the latent representation Hansen et al. (2024; 2022), inherently making the world model task-specific. In this work, we aim to decouple task-dependent information from latent-space prediction, striving to develop a versatile and task-agnostic world model capable of generalizing across different scenarios.

**Generative Models as World Models:** With the recent excitement of large scale foundation models, there have been initiatives on building large-scale video generation world models conditioned on agent’s actions in the domain of self-driving Hu et al. (2023), control Yang et al. (2023); Bruce et al. (2024), and general-purpose video generation Liu et al. (2024). These models aim to generate video predictions conditioned on text or high-level action sequences. While these models have demonstrated utility in downstream tasks like data augmentations, their reliance on language conditioning limits their application when precise visually indicative goals need to be reached. Additionally, the use of diffusion models for video generation makes them computationally expensive, further restricting their applicability for test-time optimization techniques such as MPC. In this work, we aim to build a world model in latent space rather than in the raw pixel space, which enables more precise planning and control.

**Pretrained Visual Representations:** Significant advancements have been made in the field of visual representation learning, where compact features that capture spatial and semantic information can be readily used for downstream tasks. Pre-trained models like ImageNet pre-trained ResNet He et al. (2016), I-JEPA Assran et al. (2023), and DINO Caron et al. (2021); Oquab et al. (2024) for images, as well as V-JEPA Bardes et al. (2024) for videos, and R3M Nair et al. (2022), MVP Xiao et al. (2022) for robotics have allowed fast adaptation to downstream tasks as they contain rich spatial and semantic information. While many of these models represent images using a single global feature, the introduction of Vision Transformers (ViTs) Dosovitskiy et al. (2021) has enabled the use of pre-trained patch features, as demonstrated by DINO Caron et al. (2021); Oquab et al. (2024). DINO employs a self-distillation loss that allows the model to learn representations effectively, capturing semantic layouts and improving spatial understanding within images. In this work, we leverage DINOV2’s patch embeddings to train our world model, and demonstrate that it serves as a versatile encoder capable of handling multiple precise tasks.

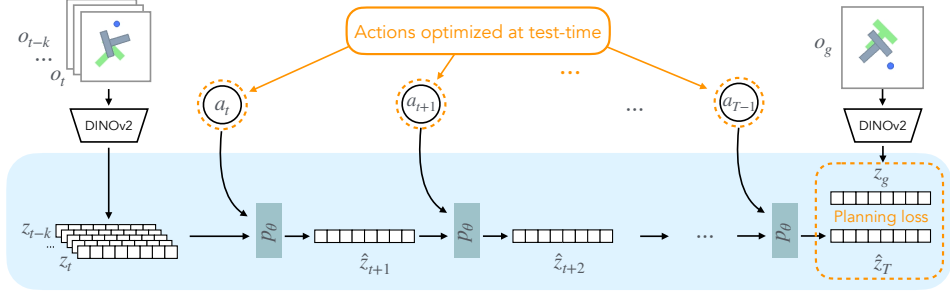


Figure 2: Architecture of DINO-WM. Given observations  $o_{t-k:t}$ , we optimize the sequence of actions  $a_{t:T-1}$  to minimize the predicted loss to the desired goal  $o_g$ . All forward computation is done in the latent space  $z$ . Here  $p_\theta$  indicates DINO-WM’s dynamics model, which is used for making future predictions.

### 3 DINO WORLD MODELS

**Overview and Problem formulation:** Our work follows the vision-based control task framework, which models the environment as a partially observable Markov decision process (POMDP). The POMDP is defined by the tuple  $(\mathcal{O}, \mathcal{A}, p)$ , where  $\mathcal{O}$  represents the observation space, and  $\mathcal{A}$  denotes the action space. The environment’s dynamics are modeled by the transition distribution  $p(o_{t+1} | o_{\leq t}, a_{\leq t})$ , which predicts future observations based on past actions and observations.

In this work, we aim to learn task-agnostic world models from pre-collected offline datasets, and use these world models to perform visual reasoning and control at test time. At test time, our system starts from an arbitrary environment state and is provided with a goal observation in the form of an RGB image, in line with prior works Wu et al. (2020); Ebert et al. (2018); Mendonca et al. (2023b), and is asked to perform a sequence of actions  $a_0, \dots, a_T$  such that the goal state can be achieved. This approach differs from world models used in online reinforcement learning (RL) where the objective is to optimize rewards for a fixed set of tasks at hand Hafner et al. (2024); Hansen et al. (2024), or from text-conditioned world models, where goals are specified through text prompts Du et al. (2023); Ko et al. (2023).

#### 3.1 DINO-BASED WORLD MODELS (DINO-WM)

We model the dynamics of the environment in the latent space. More specifically, at each time step  $t$ , our world model consists of the following components:

$$\begin{aligned} \text{Observation model: } & z_t \sim \text{enc}_\theta(z_t | o_t) \\ \text{Transition model: } & z_{t+1} \sim p_\theta(z_{t+1} | z_{t-H:t}, a_{t-H:t}) \\ \text{Decoder model (optional for visualization): } & \hat{o}_t \sim q_\theta(o_t | z_t) \end{aligned}$$

where the observation model encodes image observations to latent states  $z_t$ , and the transition model takes in a history of past latent states of length  $H$ . The decoder model takes in a latent  $z_t$ , and reconstruct the image observation  $o_t$ . We use  $\theta$  to denote the parameters of these models. Note that our decoder is entirely optional, as the training objectives for the decoder is independent for training the rest part of the world model. This eliminates the need to reconstructing images both during training and testing, which reduces computational costs compared to otherwise coupling together the training of the observational model and the decoder, as in Hafner et al. (2024); Micheli et al. (2023).

DINO-WM models only the information available from offline trajectory data in an environment, in contrast to recent online RL world models that also require task-relevant information, such as rewards Hansen et al. (2022; 2024); Hafner et al. (2020), discount factors Hafner et al. (2022); Robine et al. (2023), and termination conditions Hafner et al. (2024); Micheli et al. (2023).

##### 3.1.1 OBSERVATION MODEL

With the goal of learning a generic world model across many environments and the real world, we argue that the observation model should 1) be task and environment independent, and 2) contain

---

rich spatial information which is crucial in navigation and manipulation tasks. Contrary to previous works where the observation model is always learned for the task at hand Hafner et al. (2024), we argue instead that it is not always possible for world models to learn an observation model from scratch when facing a new environment, as perception is a general task that can be learned from the large corpus of internet data. Therefore, we choose the out-of-the-box pre-trained DINOv2 model as our world model’s observation model, as it has been shown to excel at object detection, semantic segmentation, and depth estimation tasks which require substantial spatial understanding. The observation model is kept frozen throughout both training and testing time. At each time step  $t$ , it encodes an image  $o_t$  to patch embeddings  $z_t \in \mathbb{R}^{N \times E}$ , where  $N$  denotes the number of patches, and  $E$  denotes the embedding dimension. This process is visualized in Figure 2.

### 3.1.2 TRANSITION MODEL

We adopt the ViT Dosovitskiy et al. (2021) architecture for the transition model as it is a natural choice for processing patch features. However, a few modifications are required to the architecture to allow for additional conditioning on proprioception and controller actions.

Our transition model takes in a history of past latent states  $z_{t-H:t-1}$  and actions  $a_{t-H:t-1}$ , where  $H$  is a hyperparameter denoting the context length of the model, and predicts the latent state at next time step  $z_t$ . To properly capture the temporal dependencies, where the world state at time  $t$  should only depend on previous observations and actions, we implement a causal attention mechanism in the ViT model, enabling the model to predict latents autoregressively at a frame level. Specifically, each patch vector  $z_t^i$  for the latent state  $z_t$  attends to  $\{z_{t-H:t-1}^i\}_{i=1}^N$ . This is different from past work IRIS Micheli et al. (2023) which similarly represent each observation as a sequence of vectors, but autoregressively predict  $z_t^i$  at a token level, attending to  $\{z_{t-H:t-1}^i\}_{i=1}^N$  as well as  $\{z_t^i\}_{i=1}^k$ . We argue that predicting at a frame level and treating patch vectors of one observation as a whole better captures global structure and temporal dynamics, modeling dependencies across the entire observation rather than isolated tokens, leading to improved temporal generalization.

To model the effect of the agent’s action to the environment, we condition the world model’s predictions on these actions. Specifically, we concatenate the  $K$ -dimensional action vector, mapped from the original action representation using a multi-layer perceptron (MLP), to each patch vector  $z_t^i$  for  $i = 1, \dots, N$ . When proprioceptive information is available, we incorporate it similarly by concatenating it to the observation latents, thereby integrating it into the latent states.

We train the world model with teacher forcing. During training, we slice the trajectories in to segments of length  $H + 1$ , and compute a latent consistency loss on each of the  $H$  predicted frames. For each frame, we compute

$$\mathcal{L}_{pred} = \|p_\theta(\text{enc}_\theta(o_{t-H:t}), \phi(a_{t-H:t})) - \text{enc}_\theta(o_{t+1})\|^2 \quad (1)$$

where  $\phi$  is the action encoder model that can map actions to higher dimensions. Note that our world model training is entirely performed in latent space, without the need to reconstruct the original pixel images.

### 3.1.3 DECODER FOR INTERPRETABILITY

To aid in visualization and interpretability, we use a stack of transposed convolution layers to decode the patch representations back to image pixels, similar as in Razavi et al. (2019). Given a pre-collected dataset, we optimize the parameters  $\theta$  of the decoder  $q_\theta$  with a simple reconstruction loss defined as:

$$\mathcal{L}_{rec} = \|q_\theta(z_t) - o_t\|^2, \quad \text{where } z_t = \text{enc}_\theta(o_t) \quad (2)$$

The training of the decoder is entirely independent of the transition model training, offering several advantages: **1)** The quality of the decoder does not affect the world model’s reasoning and planning capabilities for solving downstream tasks, and **2)** During planning, there is no need to reconstruct raw pixel images, thereby reducing computational costs. Nevertheless, the decoder remains valuable as it enhances the interpretability of the world model’s predictions.

## 3.2 VISUAL PLANNING WITH DINO-WM

Arguably, to evaluate the quality of the world model, it needs to be able to allow for downstream reasoning and planning. A standard evaluation metric is to perform trajectory optimization at test time

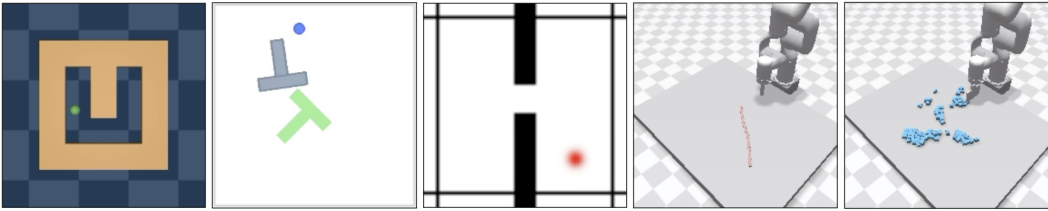


Figure 3: We evaluate DINO-WM on 5 environment suites, from left to right: PointMaze, Push-T, Two Room, Rope Manipulation, and Granular Manipulation.

with these world models and measure the performance. While the planning methods themselves are fairly standard, it serves as a means to emphasize the quality of the world models. For this purpose, our world model receives the current observation  $o_0$  and a goal observation  $o_g$ , both represented as RGB images. We formulate planning as the process of searching for a sequence of actions that the agent would take to reach  $o_g$ . To achieve this, we employ model predictive control (MPC), which facilitates planning by considering the outcomes of future actions.

We utilize the cross-entropy method (CEM), a stochastic optimization algorithm, to optimize the sequence of actions at each iteration. The planning cost is defined as the mean squared error (MSE) between the current latent state and the goal’s latent state, given by

$$\mathcal{C} = \|\hat{z}_T - z_g\|^2, \quad \text{where } \hat{z}_t = p(\hat{z}_{t-1}, a_{t-1}), \quad \hat{z}_0 = \text{enc}(o_0), \quad z_g = \text{enc}(o_g).$$

The MPC framework and CEM optimization procedure is detailed in Appendix A.4.1. Since our world model is differentiable, a possibly more efficient approach is to optimize this objective through gradient descent (GD), allowing the world model to directly guide the agent toward a specific goal. The details of GD are provided in Appendix A.4.2. However, we empirically observe that CEM outperforms GD in our experiments. We hypothesize this is due to our choice to not constrain the terrain smoothness of the world model during training, potentially leading to issues with the gradient. Full results for both planners can be found in Appendix A.4.3.

## 4 EXPERIMENTS

Our experiments are designed to address the following key questions: **1)** Can we effectively train DINO-WM using pre-collected offline datasets? **2)** Once trained, can DINO-WM be used for visual planning? **3)** To what extent does the quality of the world model depend on pre-trained visual representations? **4)** Does DINO-WM generalize to new configurations, such as variations in spatial layouts and object arrangements? To answer these questions, we train and evaluate DINO-WM across five environment suites (full description in Appendix A.1) and compare it to a variety of state-of-the-art world models that model the world both in latent space and in raw pixel space.

### 4.1 ENVIRONMENTS AND TASKS

We consider five environment suites in our evaluations spanning simple navigation environments and manipulation environments with varying dynamics complexity. For all environments, the observation space is RGB images of size (224, 224).

- a) **Point Maze:** A simple 2D point maze navigation environment in the D4RL suite Fu et al. (2021). A point agent with 2-dimensional action space moves in a U-shape maze. The agent’s dynamics incorporate physical properties such as velocity, acceleration, and inertia, making the movement realistic. The objective of the task is to navigate the maze and reach arbitrary goal locations from arbitrary starting location.
- b) **Push-T:** This manipulation environment was introduced in Chi et al. (2024) to study precise manipulation. The environment features a pusher agent interacting with a T-shaped block. The goal is to guide both the agent and the T-block from a randomly initialized state to a known feasible target configuration within 25 steps. The task requires both the agent and the T to match the target locations. Unlike previous setups, the fixed green T no longer represents the

target position for the T-block but serves purely as a visual anchor for reference. Success requires precise understanding of the contact-rich dynamics between the agent and the object, making it a challenging test for visuomotor control and object manipulation. We also introduce a variant of this where we have multiple object shapes.

- c) **Wall:** This custom 2D navigation environment featuring two rooms separated by a wall with a door opening. The task requires the agent to navigate from a randomized starting location in one room to a goal in the other room, which requires the agent to pass through the door. We introduce a variant of this environment where the positions of the wall and door are randomized to assess the model’s ability to generalize to novel configurations of familiar environment dynamics.
- d) **Rope Manipulation:** This task is simulated with Nvidia Flex Zhang et al. (2024) and consists of an XArm interacting with a rope placed on a tabletop. The objective is to move the rope from an arbitrary start configuration to a specified goal configuration.
- e) **Granular Manipulation:** Granular manipulation uses the same setting as Rope manipulation and manipulates about a hundred particles to form desired shapes.

## 4.2 BASELINES

We compare DINO-WM with the following state-of-the-art models commonly used for control:

- a) **IRIS Micheli et al. (2023):** IRIS employs a discrete autoencoder to translate visual inputs into tokens, and a GPT Transformer that predicts tokens of future observations. It combines these components to learn policies and value functions through imaginative procedures.
- b) **DreamerV3 Hafner et al. (2024):** DreamerV3 learns a world model to interpret visual inputs into categorical representation. It predicts future representations and rewards based on given action and trains an actor-critic policy from its imagined trajectories.
- c) **TD-MPC2 Hansen et al. (2024) :** TD-MPC2 learns a decoder-free world model in latent space and uses reward signals to optimize the latents. It serves as a strong baseline for reconstruction-free world modeling.
- d) **AVDC Ko et al. (2023):** AVDC leverages a diffusion model to generate an imagined video of task execution based on initial observation and a textual goal description. It then estimates optical flow between frames to capture object movements and generates robot arm commands.

## 4.3 OPTIMIZING BEHAVIORS WITH DINO-WM

With a trained world model, we study if DINO-WM be used for zero-shot planning directly in the latent space.

For the PointMaze, Push-T, and Wall environments, we sample 50 initial and goal states to measure the success rate across all instances. Due to the environment stepping time for the Rope and Granular environments, we evaluate the Chamfer Distance (CD) on 10 instances for them. In the Granular environment, we sample a random configuration from the validation set, with the goal of pushing the materials into a square shape at a randomly selected location and scale.

Table 1: Planning results for offline world models on five control environments.

Model	PointMaze SR $\uparrow$	PushT SR $\uparrow$	Wall SR $\uparrow$	Rope CD $\downarrow$	Granular CD $\downarrow$
IRIS	0.74	0.32	0.04	1.11	0.37
DreamerV3	<b>1.00</b>	0.04	<b>1.00</b>	2.49	1.05
TD-MPC2	0.00	0.00	0.00	2.52	1.21
Ours	0.98	<b>0.90</b>	0.96	<b>0.41</b>	<b>0.26</b>

As seen in Table 1, on simpler environments such as Wall and PointMaze, DINO-WM is on par with state-of-art world models like DreamerV3. However, DINO-WM significantly outperforms prior work at manipulation environments where rich contact information and object dynamics need to be accurately inferred for task completion. We notice that for TD-MPC2, the lack of reward

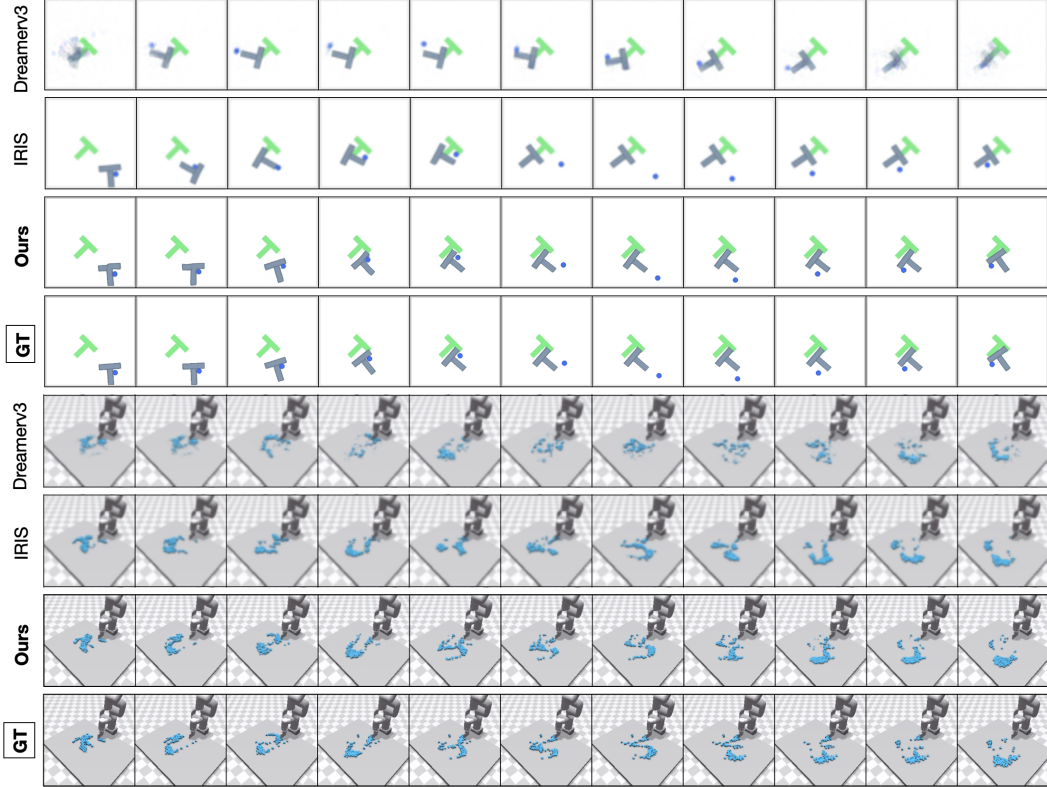


Figure 4: Openloop rollout of world models trained with various pre-trained encoders on Push-T and Granular environment. For each trajectory, the model is given the first frame as well as sequence of actions. The world models performs openloop rollout with these actions, and the images are reconstructed by a pre-trained decoder. For each environment, the bottom row denotes the ground truth. DINO-WM (Ours) rollouts are bolded and are visually indistinguishable from the ground truth observations.

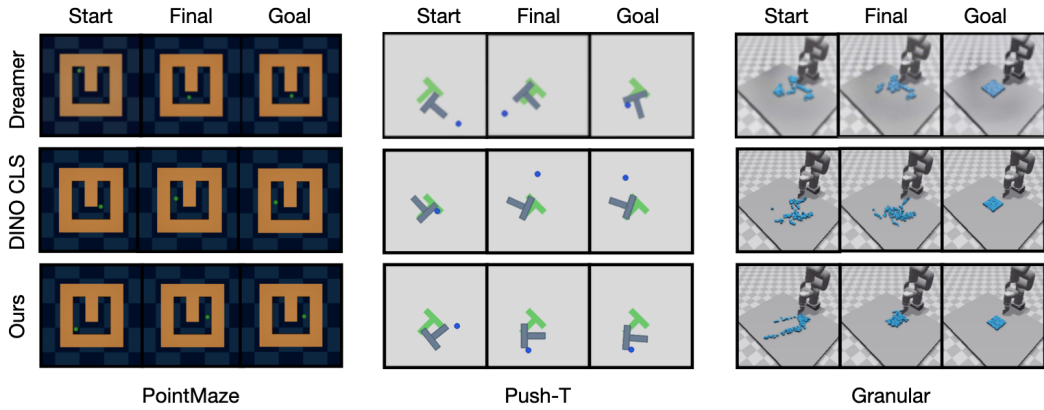


Figure 5: Planning visualizations for PointMaze, Push-T, and Granular, on randomly sampled initial and goal configurations. The task is defined by Start and Goal, denoting the initial and goal observations. Final shows the final state the system arrives at after planning with each world model. For comparison, we show the best performing world models DINO CLS and DreamerV3.

signal makes it difficult to learn good latent representations, which subsequently results in poor performance. Visualizations of some planning results can be found in Figure 5.

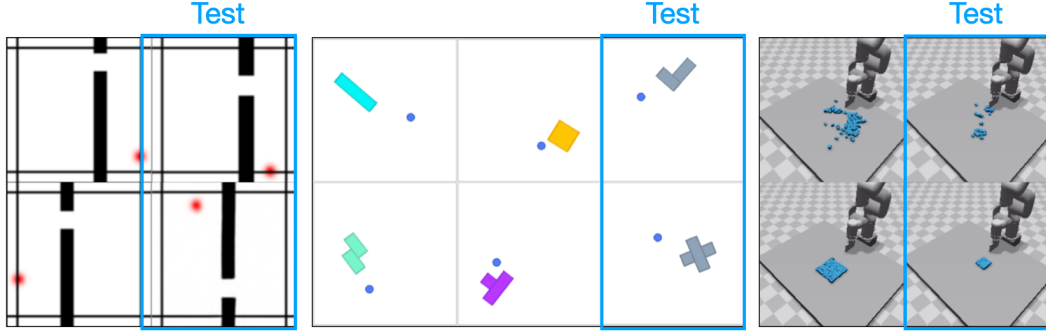


Figure 6: Training and testing visualizations for WallRandom, PushObj and GranularRandom. Test setups are highlighted in blue boxes, showcasing unseen configurations for assessing the model’s generalization ability.

#### 4.4 DOES PRE-TRAINED VISUAL REPRESENTATIONS MATTER?

We use different pre-trained general-purpose encoders as the observation model of the world model, and evaluate their downstream planning performance. Specifically, we use the following encoders commonly used in robotics control and general perception: R3M Nair et al. (2022), ImageNet pre-trained ResNet-18 Russakovsky et al. (2015); He et al. (2016) and DINO CLS Caron et al. (2021). Detailed descriptions of these encoders are in Appendix A.3.

Table 2: Planning results for world models with various pre-trained encoders.

Model	PointMaze SR $\uparrow$	PushT SR $\uparrow$	Wall SR $\uparrow$	Rope CD $\downarrow$	Granular CD $\downarrow$
R3M	0.94	0.42	0.34	1.13	0.95
ResNet	<b>0.98</b>	0.2	0.12	1.08	0.90
DINO CLS	0.96	0.44	0.58	0.84	0.79
DINOPatch (Ours)	<b>0.98</b>	<b>0.90</b>	<b>0.96</b>	<b>0.41</b>	<b>0.26</b>

In the PointMaze task, which involves simple dynamics and control, we observe that world models with various observation encoders all achieve near-perfect success rates. However, as the environment’s complexity increases—requiring more precise control and spatial understanding—world models that encode observations as a single latent vector show a significant drop in performance. We posit that patch-based representations better capture spatial information, in contrast to models like R3M, ResNet, and DINO CLS, which reduce observations to a single global feature vector, losing crucial spatial details necessary for manipulation tasks.

#### 4.5 GENERALIZING TO NOVEL ENVIRONMENT CONFIGURATIONS

We would like to measure the generalization capability of our world models not just across different goals in an environment, but across different environments themselves. For this we construct three families of environments, where the world model will be deployed in an unseen environment for unseen goals. Our families of environments consist of WallRandom, PushObj, and GranularRandom with detailed descriptions in Appendix A.2. Visualizations of training and testing examples are shown in Figure 6.

From Table 3, we observe that DINO-WM demonstrates significantly better performance in the WallRandom environment, indicating that the world model has effectively learned the general concepts of walls and doors, even when they are positioned in locations unseen during training. In contrast, other methods struggle to accurately identify the door’s position and navigate through it. The PushObj task remains challenging for all methods, as the model was only trained on the four object shapes, which makes it difficult to infer physical parameters like the center of gravity and inertia precisely. In GranularRandom, the agent encounters fewer than half the particles present during training, resulting in out-of-distribution images compared to the training instances. Nevertheless,

Table 3: Planning results for offline world models on three suites with unseen environment configurations.

Model	WallRandom	PushObj	GranularRandom
	SR $\uparrow$	SR $\uparrow$	CD $\downarrow$
IRIS	0.06	0.14	0.86
Dreamerv3	0.76	0.18	1.53
R3M	0.40	0.16	1.12
ResNet	0.40	0.14	0.98
DINO CLS	0.64	0.18	1.36
Ours	<b>0.82</b>	<b>0.34</b>	<b>0.63</b>



Figure 7: Comparison of plans generated by DINO-WM and AVDC, a diffusion-based generative model.

DINO-WM accurately encodes the scene and successfully gathers the particles into a designated square location with the lowest Chamfer Distance (CD) compared to the baselines, demonstrating better scene understanding. We hypothesize that this is due to DINO-WM’s observation model encoding the scene as patch features, making the variance in particle number still within the distribution for each image patch.

#### 4.6 QUALITATIVE COMPARISONS WITH GENERATIVE VIDEO MODELS

Given the prominence of generative video models, it is reasonable to presume that they could readily serve as world models. To investigate the usefulness of DINO-WM over such video generative models, we compare it with imagined rollouts from AVDC Ko et al. (2023), a diffusion-based generative model. As seen in Figure 7, we find that the diffusion model trained on benchmarks produce future images that are mostly visually realistic, however they are not physically plausible as we can see that large changes can occur in a single timestep of prediction, and may have difficulties in reaching to the exact goal state. Potentially stronger generative models in the future could alleviate this issue.

We also compare DINO-WM with a variant of AVDC, where the diffusion model is trained to generate the next observation  $o_{t+1}$  conditioned on the current observation  $o_t$  and action  $a_t$ , rather than generating an entire sequence of observations at once conditioned on a text goal. As detailed in Appendix A.5, it can be seen that the action-conditioned diffusion model diverges from the ground truth observations over long-term predictions, making it insufficient for accurate task planning.

#### 4.7 DECODING AND INTERPRETING THE LATENTS

Although DINO-WM operates in latent space and the observation model is not trained with pixel reconstruction objectives, training a decoder is still valuable for interpreting the model’s predictions. We evaluate the image quality of predicted futures across all models and find that our approach outperforms others, even those whose encoders are trained with environment-specific reconstruction objectives. We show openloop rollout visualizations in Figure 4. This demonstrates the robustness of DINO-WM despite the lack of explicit pixel-level supervision. We report two key metrics: Structural Similarity Index (SSIM) Wang et al. (2004) and Learned Perceptual Image Patch Similarity (LPIPS) Zhang et al. (2018) on the reconstruction of world models’ predicted future states.

---

SSIM measures the perceived quality of images by evaluating structural information and luminance consistency between predicted and ground-truth images, with higher values indicating greater similarity. LPIPS, on the other hand, assesses perceptual similarity by comparing deep representations of images, with lower scores reflecting closer visual similarity.

Table 4: Comparison of world models across different environments on LPIPS and SSIM metrics.

<b>Method</b>	LPIPS ↓				SSIM ↑			
	<b>PushT</b>	<b>Wall</b>	<b>Rope</b>	<b>Granular</b>	<b>PushT</b>	<b>Wall</b>	<b>Rope</b>	<b>Granular</b>
R3M	0.045	0.0083	0.023	0.08	0.956	0.994	0.982	0.917
ResNet	0.063	0.0024	0.025	0.08	0.950	0.996	0.980	0.915
DinoCLS	0.039	0.004	0.029	0.086	0.973	0.996	0.980	0.912
AVDC	0.046	0.030	0.060	0.106	0.959	0.983	0.979	0.909
Ours	<b>0.007</b>	<b>0.0016</b>	<b>0.009</b>	<b>0.035</b>	<b>0.985</b>	<b>0.997</b>	<b>0.985</b>	<b>0.940</b>

## 5 CONCLUSION, LIMITATIONS & FUTURE WORK

In this work, we introduce DINO-WM, a simple yet effective technique for modeling visual dynamics in latent space without the need for pixel-space reconstruction. We have demonstrated that DINO-WM captures environmental dynamics and generalizes to unseen configurations, independent of task specifications, enabling visual reasoning at test time and generating zero-shot solutions for downstream tasks through planning. DINO-WM takes a step toward bridging the gap between task-agnostic world modeling and reasoning and control, offering promising prospects for generic world models in real-world applications. For limitations, DINO-WM still relies on the availability of ground truth actions from agents, which may not always be feasible when training with vast video data from the internet. Additionally, while we currently plan in action space for downstream task solving, an extension of this work could involve developing a hierarchical structure that integrates high-level planning with low-level control policies to enable solving more fine-grained control tasks.

---

## ETHICS STATEMENT

This work explores creation of latent world models that can be used for better downstream planning. While we do not anticipate a potential for current misuse as this particular work, we can imagine future work that builds on this can lead to impact in robotics. Such potential applications to robotics open up a potential to misuse, which we acknowledge.

## REPRODUCIBILITY STATEMENT

All code, models, and benchmarks produced from this project will be made open-source on our project website. We also provide thorough textual descriptions of all experimental procedures in the Appendix. Appendix A.1 describes our environments, data generation, and task definitions. In Appendix A.4, we outline all the planning optimization methods that we used in this paper. We provide further comparisons for DINO-WM and using generative models as world models in Appendix A.5, and additional planning visualizations with DINO-WM in Appendix A.7. Finally, Appendix A.6 provides the hyperparameters we used for training the world model for reproducing our experiment results in Section 4.1.

## REFERENCES

- Ananye Agarwal, Ashish Kumar, Jitendra Malik, and Deepak Pathak. Legged locomotion in challenging terrains using egocentric vision, 2022. URL <https://arxiv.org/abs/2211.07638>.
- Mahmoud Assran, Quentin Duval, Ishan Misra, Piotr Bojanowski, Pascal Vincent, Michael Rabbat, Yann LeCun, and Nicolas Ballas. Self-supervised learning from images with a joint-embedding predictive architecture. In *Proceedings of the IEEE/CVF Conference on Computer Vision and Pattern Recognition*, pp. 15619–15629, 2023.
- Alessandro Astolfi, Dimitrios Karagiannis, and Romeo Ortega. *Nonlinear and adaptive control with applications*, volume 187. Springer, 2008.
- Adrien Bardes, Quentin Garrido, Jean Ponce, Xinlei Chen, Michael Rabbat, Yann LeCun, Mido Assran, and Nicolas Ballas. V-JEPA: Latent video prediction for visual representation learning, 2024. URL <https://openreview.net/forum?id=WFYbBOEOtv>.
- Anthony Brohan, Noah Brown, Justice Carbajal, Yevgen Chebotar, Xi Chen, Krzysztof Choromanski, Tianli Ding, Danny Driess, Avinava Dubey, Chelsea Finn, Pete Florence, Chuyuan Fu, Montse Gonzalez Arenas, Keerthana Gopalakrishnan, Kehang Han, Karol Hausman, Alexander Herzog, Jasmine Hsu, Brian Ichter, Alex Irpan, Nikhil Joshi, Ryan Julian, Dmitry Kalashnikov, Yuheng Kuang, Isabel Leal, Lisa Lee, Tsang-Wei Edward Lee, Sergey Levine, Yao Lu, Henryk Michalewski, Igor Mordatch, Karl Pertsch, Kanishka Rao, Krista Reymann, Michael Ryoo, Grecia Salazar, Pannag Sanketi, Pierre Sermanet, Jaspia Singh, Anikait Singh, Radu Soricu, Huong Tran, Vincent Vanhoucke, Quan Vuong, Ayzaan Wahid, Stefan Welker, Paul Wohlhart, Jialin Wu, Fei Xia, Ted Xiao, Peng Xu, Sichun Xu, Tianhe Yu, and Brianna Zitkovich. Rt-2: Vision-language-action models transfer web knowledge to robotic control, 2023a. URL <https://arxiv.org/abs/2307.15818>.
- Anthony Brohan, Noah Brown, Justice Carbajal, Yevgen Chebotar, Joseph Dabis, Chelsea Finn, Keerthana Gopalakrishnan, Karol Hausman, Alex Herzog, Jasmine Hsu, Julian Ibarz, Brian Ichter, Alex Irpan, Tomas Jackson, Sally Jesmonth, Nikhil J Joshi, Ryan Julian, Dmitry Kalashnikov, Yuheng Kuang, Isabel Leal, Kuang-Huei Lee, Sergey Levine, Yao Lu, Utsav Malla, Deeksha Manjunath, Igor Mordatch, Ofir Nachum, Carolina Parada, Jodilyn Peralta, Emily Perez, Karl Pertsch, Jornell Quiambao, Kanishka Rao, Michael Ryoo, Grecia Salazar, Pannag Sanketi, Kevin Sayed, Jaspia Singh, Sumedh Sontakke, Austin Stone, Clayton Tan, Huong Tran, Vincent Vanhoucke, Steve Vega, Quan Vuong, Fei Xia, Ted Xiao, Peng Xu, Sichun Xu, Tianhe Yu, and Brianna Zitkovich. Rt-1: Robotics transformer for real-world control at scale, 2023b. URL <https://arxiv.org/abs/2212.06817>.

- 
- Jake Bruce, Michael Dennis, Ashley Edwards, Jack Parker-Holder, Yuge Shi, Edward Hughes, Matthew Lai, Aditi Mavalankar, Richie Steigerwald, Chris Apps, Yusuf Aytar, Sarah Bechtle, Feryal Behbahani, Stephanie Chan, Nicolas Heess, Lucy Gonzalez, Simon Osindero, Sherjil Ozair, Scott Reed, Jingwei Zhang, Konrad Zolna, Jeff Clune, Nando de Freitas, Satinder Singh, and Tim Rocktäschel. Genie: Generative interactive environments, 2024. URL <https://arxiv.org/abs/2402.15391>.
- Mathilde Caron, Hugo Touvron, Ishan Misra, Hervé Jégou, Julien Mairal, Piotr Bojanowski, and Armand Joulin. Emerging properties in self-supervised vision transformers, 2021. URL <https://arxiv.org/abs/2104.14294>.
- Cheng Chi, Zhenjia Xu, Siyuan Feng, Eric Cousineau, Yilun Du, Benjamin Burchfiel, Russ Tedrake, and Shuran Song. Diffusion policy: Visuomotor policy learning via action diffusion, 2024. URL <https://arxiv.org/abs/2303.04137>.
- Kurtland Chua, Roberto Calandra, Rowan McAllister, and Sergey Levine. Deep reinforcement learning in a handful of trials using probabilistic dynamics models, 2018. URL <https://arxiv.org/abs/1805.12114>.
- Marc Peter Deisenroth and Carl Edward Rasmussen. Pilco: A model-based and data-efficient approach to policy search. In *International Conference on Machine Learning*, 2011. URL <https://api.semanticscholar.org/CorpusID:14273320>.
- Alexey Dosovitskiy, Lucas Beyer, Alexander Kolesnikov, Dirk Weissenborn, Xiaohua Zhai, Thomas Unterthiner, Mostafa Dehghani, Matthias Minderer, Georg Heigold, Sylvain Gelly, Jakob Uszkoreit, and Neil Houlsby. An image is worth 16x16 words: Transformers for image recognition at scale, 2021. URL <https://arxiv.org/abs/2010.11929>.
- Yilun Du, Mengjiao Yang, Bo Dai, Hanjun Dai, Ofir Nachum, Joshua B. Tenenbaum, Dale Schuurmans, and Pieter Abbeel. Learning universal policies via text-guided video generation, 2023. URL <https://arxiv.org/abs/2302.00111>.
- Frederik Ebert, Chelsea Finn, Sudeep Dasari, Annie Xie, Alex Lee, and Sergey Levine. Visual foresight: Model-based deep reinforcement learning for vision-based robotic control, 2018. URL <https://arxiv.org/abs/1812.00568>.
- Haritheja Etukuru, Norihito Naka, Zijin Hu, Seungjae Lee, Julian Mehu, Aaron Edsinger, Chris Paxton, Soumith Chintala, Lerrel Pinto, and Nur Muhammad Mahi Shafiullah. Robot utility models: General policies for zero-shot deployment in new environments. *arXiv preprint arXiv:2409.05865*, 2024.
- Chelsea Finn and Sergey Levine. Deep visual foresight for planning robot motion, 2017. URL <https://arxiv.org/abs/1610.00696>.
- Justin Fu, Aviral Kumar, Ofir Nachum, George Tucker, and Sergey Levine. D4rl: Datasets for deep data-driven reinforcement learning, 2021. URL <https://arxiv.org/abs/2004.07219>.
- David Ha and Jürgen Schmidhuber. World models. 2018. doi: 10.5281/ZENODO.1207631. URL <https://zenodo.org/record/1207631>.
- Danijar Hafner, Timothy Lillicrap, Ian Fischer, Ruben Villegas, David Ha, Honglak Lee, and James Davidson. Learning latent dynamics for planning from pixels, 2019. URL <https://arxiv.org/abs/1811.04551>.
- Danijar Hafner, Timothy Lillicrap, Jimmy Ba, and Mohammad Norouzi. Dream to control: Learning behaviors by latent imagination, 2020. URL <https://arxiv.org/abs/1912.01603>.
- Danijar Hafner, Timothy Lillicrap, Mohammad Norouzi, and Jimmy Ba. Mastering atari with discrete world models, 2022. URL <https://arxiv.org/abs/2010.02193>.
- Danijar Hafner, Jurgis Pasukonis, Jimmy Ba, and Timothy Lillicrap. Mastering diverse domains through world models, 2024. URL <https://arxiv.org/abs/2301.04104>.

- 
- Siddhant Haldar, Zhuoran Peng, and Lerrel Pinto. Baku: An efficient transformer for multi-task policy learning, 2024. URL <https://arxiv.org/abs/2406.07539>.
- Nicklas Hansen, Xiaolong Wang, and Hao Su. Temporal difference learning for model predictive control, 2022. URL <https://arxiv.org/abs/2203.04955>.
- Nicklas Hansen, Hao Su, and Xiaolong Wang. Td-mpc2: Scalable, robust world models for continuous control, 2024. URL <https://arxiv.org/abs/2310.16828>.
- Kaiming He, Xiangyu Zhang, Shaoqing Ren, and Jian Sun. Deep residual learning for image recognition. In *Proceedings of the IEEE conference on computer vision and pattern recognition*, pp. 770–778, 2016.
- KS Holkar and Laxman M Waghmare. An overview of model predictive control. *International Journal of control and automation*, 3(4):47–63, 2010.
- Anthony Hu, Lloyd Russell, Hudson Yeo, Zak Murez, George Fedoseev, Alex Kendall, Jamie Shotton, and Gianluca Corrado. Gaia-1: A generative world model for autonomous driving, 2023.
- Po-Chen Ko, Jiayuan Mao, Yilun Du, Shao-Hua Sun, and Joshua B. Tenenbaum. Learning to act from actionless videos through dense correspondences, 2023. URL <https://arxiv.org/abs/2310.08576>.
- Seungjae Lee, Yibin Wang, Haritheja Etukuru, H. Jin Kim, Nur Muhammad Mahi Shafiullah, and Lerrel Pinto. Behavior generation with latent actions, 2024. URL <https://arxiv.org/abs/2403.03181>.
- Ian Lenz, Ross A. Knepper, and Ashutosh Saxena. Deepmpc: Learning deep latent features for model predictive control. In *Robotics: Science and Systems*, 2015. URL <https://api.semanticscholar.org/CorpusID:10130184>.
- Yixin Liu, Kai Zhang, Yuan Li, Zhiling Yan, Chujie Gao, Ruoxi Chen, Zhengqing Yuan, Yue Huang, Hanchi Sun, Jianfeng Gao, Lifang He, and Lichao Sun. Sora: A review on background, technology, limitations, and opportunities of large vision models, 2024. URL <https://arxiv.org/abs/2402.17177>.
- Yecheng Jason Ma, William Liang, Guanzhi Wang, De-An Huang, Osbert Bastani, Dinesh Jayaraman, Yuke Zhu, Linxi Fan, and Anima Anandkumar. Eureka: Human-level reward design via coding large language models, 2024. URL <https://arxiv.org/abs/2310.12931>.
- Russell Mendonca, Oleh Rybkin, Kostas Daniilidis, Danijar Hafner, and Deepak Pathak. Discovering and achieving goals via world models, 2021. URL <https://arxiv.org/abs/2110.09514>.
- Russell Mendonca, Shikhar Bahl, and Deepak Pathak. Alan: Autonomously exploring robotic agents in the real world, 2023a. URL <https://arxiv.org/abs/2302.06604>.
- Russell Mendonca, Shikhar Bahl, and Deepak Pathak. Structured world models from human videos, 2023b. URL <https://arxiv.org/abs/2308.10901>.
- Vincent Micheli, Eloi Alonso, and François Fleuret. Transformers are sample-efficient world models, 2023. URL <https://arxiv.org/abs/2209.00588>.
- Anusha Nagabandi, Kurt Konoglie, Sergey Levine, and Vikash Kumar. Deep dynamics models for learning dexterous manipulation, 2019. URL <https://arxiv.org/abs/1909.11652>.
- Suraj Nair, Aravind Rajeswaran, Vikash Kumar, Chelsea Finn, and Abhinav Gupta. R3m: A universal visual representation for robot manipulation, 2022. URL <https://arxiv.org/abs/2203.12601>.
- Maxime Oquab, Timothée Darcet, Théo Moutakanni, Huy Vo, Marc Szafraniec, Vasil Khalidov, Pierre Fernandez, Daniel Haziza, Francisco Massa, Alaaeldin El-Nouby, Mahmoud Assran, Nicolas Ballas, Wojciech Galuba, Russell Howes, Po-Yao Huang, Shang-Wen Li, Ishan Misra, Michael Rabbat, Vasu Sharma, Gabriel Synnaeve, Hu Xu, Hervé Jegou, Julien Mairal, Patrick Labatut, Armand Joulin, and Piotr Bojanowski. Dinov2: Learning robust visual features without supervision, 2024. URL <https://arxiv.org/abs/2304.07193>.

- 
- Deepak Pathak, Parsa Mahmoudieh, Guanghao Luo, Pulkit Agrawal, Dian Chen, Yide Shentu, Evan Shelhamer, Jitendra Malik, Alexei A. Efros, and Trevor Darrell. Zero-shot visual imitation, 2018. URL <https://arxiv.org/abs/1804.08606>.
- Ali Razavi, Aaron van den Oord, and Oriol Vinyals. Generating diverse high-fidelity images with vq-vae-2, 2019. URL <https://arxiv.org/abs/1906.00446>.
- Scott Reed, Konrad Zolna, Emilio Parisotto, Sergio Gomez Colmenarejo, Alexander Novikov, Gabriel Barth-Maron, Mai Gimenez, Yury Sulsky, Jackie Kay, Jost Tobias Springenberg, Tom Eccles, Jake Bruce, Ali Razavi, Ashley Edwards, Nicolas Heess, Yutian Chen, Raia Hadsell, Oriol Vinyals, Mahyar Bordbar, and Nando de Freitas. A generalist agent, 2022. URL <https://arxiv.org/abs/2205.06175>.
- Jan Robine, Marc Höftmann, Tobias Uelwer, and Stefan Harmeling. Transformer-based world models are happy with 100k interactions, 2023. URL <https://arxiv.org/abs/2303.07109>.
- Olga Russakovsky, Jia Deng, Hao Su, Jonathan Krause, Sanjeev Satheesh, Sean Ma, Zhiheng Huang, Andrej Karpathy, Aditya Khosla, Michael Bernstein, Alexander C. Berg, and Li Fei-Fei. Imagenet large scale visual recognition challenge, 2015. URL <https://arxiv.org/abs/1409.0575>.
- Ramanan Sekar, Oleh Rybkin, Kostas Daniilidis, Pieter Abbeel, Danijar Hafner, and Deepak Pathak. Planning to explore via self-supervised world models, 2020. URL <https://arxiv.org/abs/2005.05960>.
- Richard S Sutton. Dyna, an integrated architecture for learning, planning, and reacting. *ACM Sigart Bulletin*, 2(4):160–163, 1991.
- Emanuel Todorov and Weiwei Li. A generalized iterative lqg method for locally-optimal feedback control of constrained nonlinear stochastic systems. In *Proceedings of the 2005, American Control Conference, 2005.*, pp. 300–306. IEEE, 2005.
- Zhou Wang, A.C. Bovik, H.R. Sheikh, and E.P. Simoncelli. Image quality assessment: from error visibility to structural similarity. *IEEE Transactions on Image Processing*, 13(4):600–612, 2004. doi: 10.1109/TIP.2003.819861.
- Chuan Wen, Xingyu Lin, John So, Kai Chen, Qi Dou, Yang Gao, and Pieter Abbeel. Any-point trajectory modeling for policy learning, 2024. URL <https://arxiv.org/abs/2401.00025>.
- Grady Williams, Nolan Wagener, Brian Goldfain, Paul Drews, James M Rehg, Byron Boots, and Evangelos A Theodorou. Information theoretic mpc for model-based reinforcement learning. In *2017 IEEE international conference on robotics and automation (ICRA)*, pp. 1714–1721. IEEE, 2017.
- Yilin Wu, Wilson Yan, Thanard Kurutach, Lerrel Pinto, and Pieter Abbeel. Learning to manipulate deformable objects without demonstrations, 2020. URL <https://arxiv.org/abs/1910.13439>.
- Tete Xiao, Ilija Radosavovic, Trevor Darrell, and Jitendra Malik. Masked visual pre-training for motor control, 2022. URL <https://arxiv.org/abs/2203.06173>.
- Wilson Yan, Ashwin Vangipuram, Pieter Abbeel, and Lerrel Pinto. Learning predictive representations for deformable objects using contrastive estimation. In *Conference on Robot Learning*, pp. 564–574. PMLR, 2021.
- Mengjiao Yang, Yilun Du, Kamyar Ghasemipour, Jonathan Tompson, Dale Schuurmans, and Pieter Abbeel. Learning interactive real-world simulators, 2023.
- Kaifeng Zhang, Baoyu Li, Kris Hauser, and Yunzhu Li. Adaptigraph: Material-adaptive graph-based neural dynamics for robotic manipulation, 2024. URL <https://arxiv.org/abs/2407.07889>.

---

Richard Zhang, Phillip Isola, Alexei A. Efros, Eli Shechtman, and Oliver Wang. The unreasonable effectiveness of deep features as a perceptual metric. *CoRR*, abs/1801.03924, 2018. URL <http://arxiv.org/abs/1801.03924>.

Tony Z. Zhao, Vikash Kumar, Sergey Levine, and Chelsea Finn. Learning fine-grained bimanual manipulation with low-cost hardware, 2023. URL <https://arxiv.org/abs/2304.13705>.

Gaoyue Zhou, Victoria Dean, Mohan Kumar Srirama, Aravind Rajeswaran, Jyothish Pari, Kyle Hatch, Aryan Jain, Tianhe Yu, Pieter Abbeel, Lerrel Pinto, Chelsea Finn, and Abhinav Gupta. Train offline, test online: A real robot learning benchmark, 2023. URL <https://arxiv.org/abs/2306.00942>.

---

## A APPENDIX

### A.1 ENVIRONMENTS AND DATASET GENERATION

- a) **Point Maze:** In this environment introduced by Fu et al. (2021), the task is for a force-actuated 2-DoF ball in the catesian directions x and y to reach a target goal. The agent’s dynamics incorporate physical properties such as velocity, acceleration, and inertia, making the movement realistic. We customize the environment by altering the maze configuration to test the model’s generalization ability in unseen situations. We generate 2000 fully random trajectories to train our world models.
- b) **Push-T:** This environment introduced by Chi et al. (2024) features a pusher agent interacting with a T-shaped block. The goal is to guide both the agent and the T-block from a randomly initialized state to a known feasible target configuration within 25 steps. The task requires both the agent and the T to match the target locations. Unlike previous setups, the fixed green T no longer represents the target position for the T-block but serves purely as a visual anchor for reference. Success requires precise understanding of the contact-rich dynamics between the agent and the object, making it a challenging test for visuomotor control and object manipulation. Additionally, we introduce variations by altering the shape and color of the object to assess the model’s capability to adapt to novel tasks. We generate a dataset of 18500 samples replayed the original released expert trajectories with various level of noise and evaluate the model’s performance across all different shapes to assess its adaptability.
- c) **Wall:** This custom 2D navigation environment features two rooms separated by a wall with a door. The agent’s task is to navigate from a randomized starting location in one room to a goal in the other, passing through the door. We present a variant where wall and door positions are randomized, testing the model’s generalization to novel configurations. For the fixed wall setting, we train on a fully random dataset of 2000 trajectories each with 50 time steps. For the variant with multiple training environment configurations, we generate 10240 random trajectories.
- d) **Rope Manipulation:** Introduced in Zhang et al. (2024), this task is simulated with Nvidia Flex Zhang et al. (2024) and consists of an XArm interacting with a soft rope placed on a tabletop. The objective is to move the rope from an arbitrary starting configuration to a goal configuration specified at inference time. For training, we generate a random dataset of 1000 trajectories of 20 time steps of random actions from random starting positions, while testing involves goal configurations set from varied initial positions, incorporating random variations in orientation and spatial displacement.
- e) **Granular Manipulation:** This environment uses the same simulation setup as Rope Manipulation and involves manipulating about a hundred particles to form desired shapes. The training data consists of 1000 trajectories of 20 time steps of random actions starting from the same initial configuration, while testing is performed on specific goal shapes from diverse starting positions, along with random variations in particle distribution, spacing, and orientation.

### A.2 ENVIRONMENT FAMILIES FOR TESTING GENERALIZATION

1. **WallRandom:** Based on the Wall environment, but with randomized wall and door positions. At test time, the task requires navigating from a random starting position on one side of the wall to a random position on the other side, with non-overlapping wall and door positions seen during training.
2. **PushObj:** Derived from the Push-T environment, where we introduce novel block shapes, including Tetris-like blocks and a "+" shape. We train the model with four shapes and evaluate on two unseen shapes. The task involves both the agent and object reaching target locations.
3. **GranularRandom:** Derived from the Granular environment, where we initialize the scene with a different amount of particles. The task requires the robot to gather all particles to a square shape at a randomly sampled location. For this task, we directly take the models that are trained with a fixed amount of materials used in Section 4.3.

---

Visualizations can be found in Figure 6.

### A.3 PRETRAINING FEATURES

- a) **R3M:** A ResNet-18 model pre-trained on a wide range of real-world human manipulation videos Nair et al. (2022).
- b) **ImageNet:** A ResNet-18 model pre-trained on the ImageNet-1K dataset Russakovsky et al. (2015).
- c) **DINO CLS:** The pre-trained DINOv2 model provides two types of embeddings: Patch and CLS. The CLS embedding is a 1-dimensional vector that encapsulates the global information of an image.

### A.4 PLANNING OPTIMIZATION

In this section, we detail the optimization procedures for planning in our experiments.

#### A.4.1 MODEL PREDICTIVE CONTROL WITH CROSS-ENTROPY METHOD

- a) Given the current observation  $o_0$  and the goal observation  $o_g$ , both represented as RGB images, the observations are first encoded into latent states:

$$\hat{z}_0 = \text{enc}(o_0), \quad z_g = \text{enc}(o_g). \quad (3)$$

- b) The planning objective is defined as the mean squared error (MSE) between the predicted latent state at the final timestep  $T$  and the goal latent state:

$$\mathcal{C} = \|\hat{z}_T - z_g\|^2, \quad \text{where } \hat{z}_t = p(\hat{z}_{t-1}, a_{t-1}), \quad \hat{z}_0 = \text{enc}(o_0). \quad (4)$$

- c) At each planning iteration, CEM samples a population of  $N$  action sequences, each of length  $T$ , from a distribution. The initial distribution is set to be Gaussian.
- d) For each sampled action sequence  $\{a_0, a_1, \dots, a_{T-1}\}$ , the world model is used to predict the resulting trajectory in the latent space:

$$\hat{z}_t = p(\hat{z}_{t-1}, a_{t-1}), \quad t = 1, \dots, T. \quad (5)$$

And the cost  $\mathcal{C}$  is calculated for each trajectory.

- e) The top  $K$  action sequences with the lowest cost are selected, and the mean and covariance of the distribution are updated accordingly.
- f) A new set of  $N$  action sequences is sampled from the updated distribution, and the process repeats until success is achieved or after a fixed number of iterations that we set as hyperparameter.
- g) After the optimization process is done, the first  $k$  actions  $a_0, \dots, a_k$  is executed in the environment. The process then repeats at the next time step with the new observation.

#### A.4.2 GRADIENT DESCENT:

Since our world model is differentiable, we also consider an optimization approach using Gradient Descent (GD) which directly minimizes the cost by optimizing the actions through backpropagation.

- a) We first encode the current observation  $o_0$  and goal observation  $o_g$  into latent spaces:

$$\hat{z}_0 = \text{enc}(o_0), \quad z_g = \text{enc}(o_g). \quad (6)$$

- b) The objective remains the same as for CEM:

$$\mathcal{C} = \|\hat{z}_T - z_g\|^2, \quad \text{where } \hat{z}_t = p(\hat{z}_{t-1}, a_{t-1}), \quad \hat{z}_0 = \text{enc}(o_0). \quad (7)$$

- c) Using the gradients of the cost with respect to the action sequence  $\{a_0, a_1, \dots, a_{T-1}\}$ , the actions are updated iteratively:

$$a_t \leftarrow a_t - \eta \frac{\partial \mathcal{C}}{\partial a_t}, \quad t = 0, \dots, T-1, \quad (8)$$

where  $\eta$  is the learning rate

- d) The process repeats until a fixed number of interactions is reached, and we execute the first  $k$  actions  $a_0, \dots, a_k$  in the environment, where  $k$  is a pre-determined hyperparameter.

#### A.4.3 PLANNING RESULTS

Here we present the full planning performance using various planning optimization methods. CEM denotes the setting where we use CEM to optimize a sequence of actions, and execute those actions in the environment without any correction or replan. Similarly, GD denotes optimizing with gradient decent and execute all planned actions at once in an open-loop way. MPC denotes allowing replan and receding horizon with CEM for optimization.

Table 5: Planning results of DINO-WM

	PointMaze	Push-T	Wall	Rope	Granular
CEM	0.8	0.86	0.74	NA	NA
GD	0.22	0.28	NA	NA	NA
MPC	0.98	0.90	0.96	0.41	0.26

#### A.5 COMPARISON WITH ACTION-CONDITIONED GENERATIVE MODELS

We compare DINO-WM with a variant of AVDC, where the diffusion model is trained to generate the next observation  $o_{t+1}$  conditioned on the current observation  $o_t$  and action  $a_t$ , rather than generating an entire sequence of observations at once conditioned on a text goal. We then present openloop rollout results on validation trajectories using this action-conditioned diffusion model, with visualizations shown in Figure 8. It can be seen that the action-conditioned diffusion model diverges from the ground truth observations over long-term predictions, making it insufficient for accurate task planning.

#### A.6 HYPERPARAMETERS AND IMPLEMENTATION

We present the DINO-WM hyperparameters and relevant implementation repos below. We train the world models for all environments with the same hyperparameters.

Table 6: Environment-dependent hyperparameters for DINO-WM training

	$H$
PointMaze	3
Push-T	3
Wall	1
Rope	1
Granular	1

Table 7: Shared hyperparameters for DINO-WM training

Name	Value
Image size	224
Optimizer	AdamW
Decoder lr	3e-4
Predictor lr	5e-5
Action encoder lr	5e-4
Action emb dim	10
Epochs	100
Batch size	32

- DINoV2: <https://github.com/facebookresearch/dinov2>
- DreamerV3: <https://github.com/NM512/dreamerv3-torch>
- AVDC: <https://github.com/flow-diffusion/AVDC>
- R3M: <https://github.com/facebookresearch/r3m/>

We base our predictor implementation on <https://github.com/lucidrains/vit-pytorch/>.

#### A.7 ADDITIONAL PLANNING VISUALIZATIONS

We present additional visualizations for planning with DINO-WM. In this setting, all planning instances share the same initial observations but have different goal observations to demonstrate

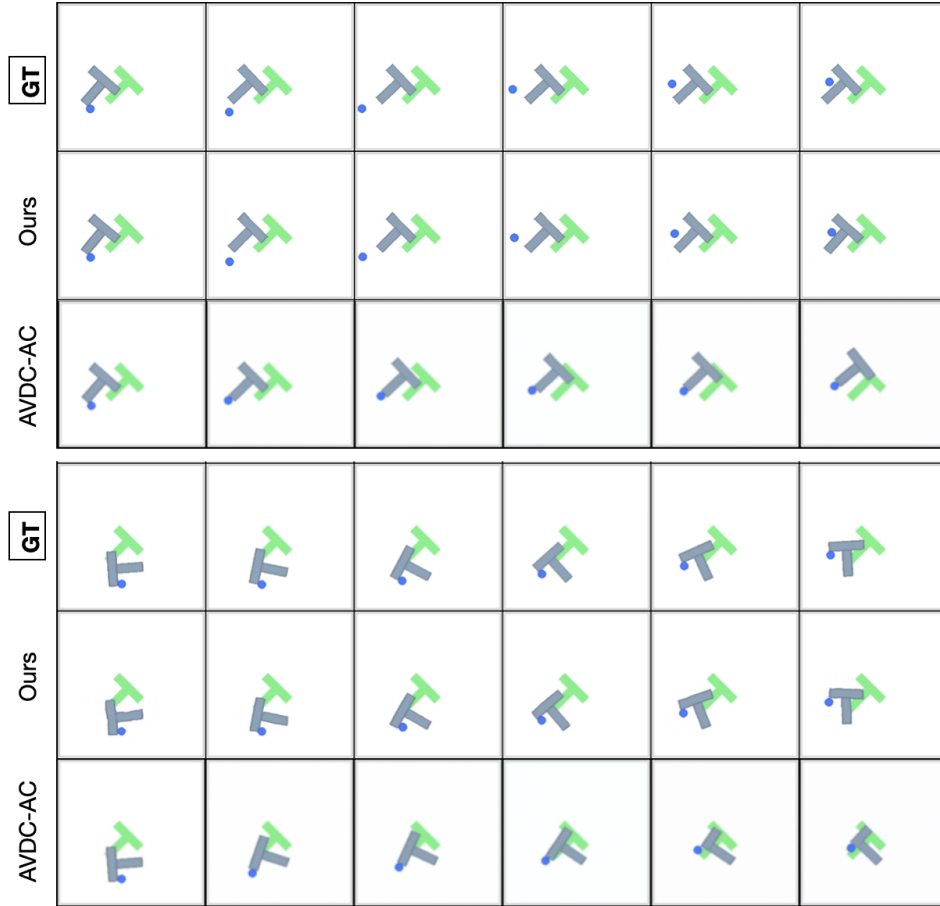


Figure 8: Openloop rollout on PushT with DINO-WM and action-conditioned AVDC (AVDC-AC). For each trajectory, the model is given the first frame as well as sequence of actions. The world models performs openloop rollout with these actions.

DINO-WM’s generalization capabilities in planning. We show trajectory pairs to compare the environment’s observations after executing a sequence of planned actions with DINO-WM’s imagined trajectories. The left-most column denotes the initial observations, and the right-most shaded column denotes the goal observations. Each pair of rows represents a planning instance: the top (shaded) row shows the environment’s observation after executing 25 planned actions, and the bottom row shows the world model’s imagined observations.

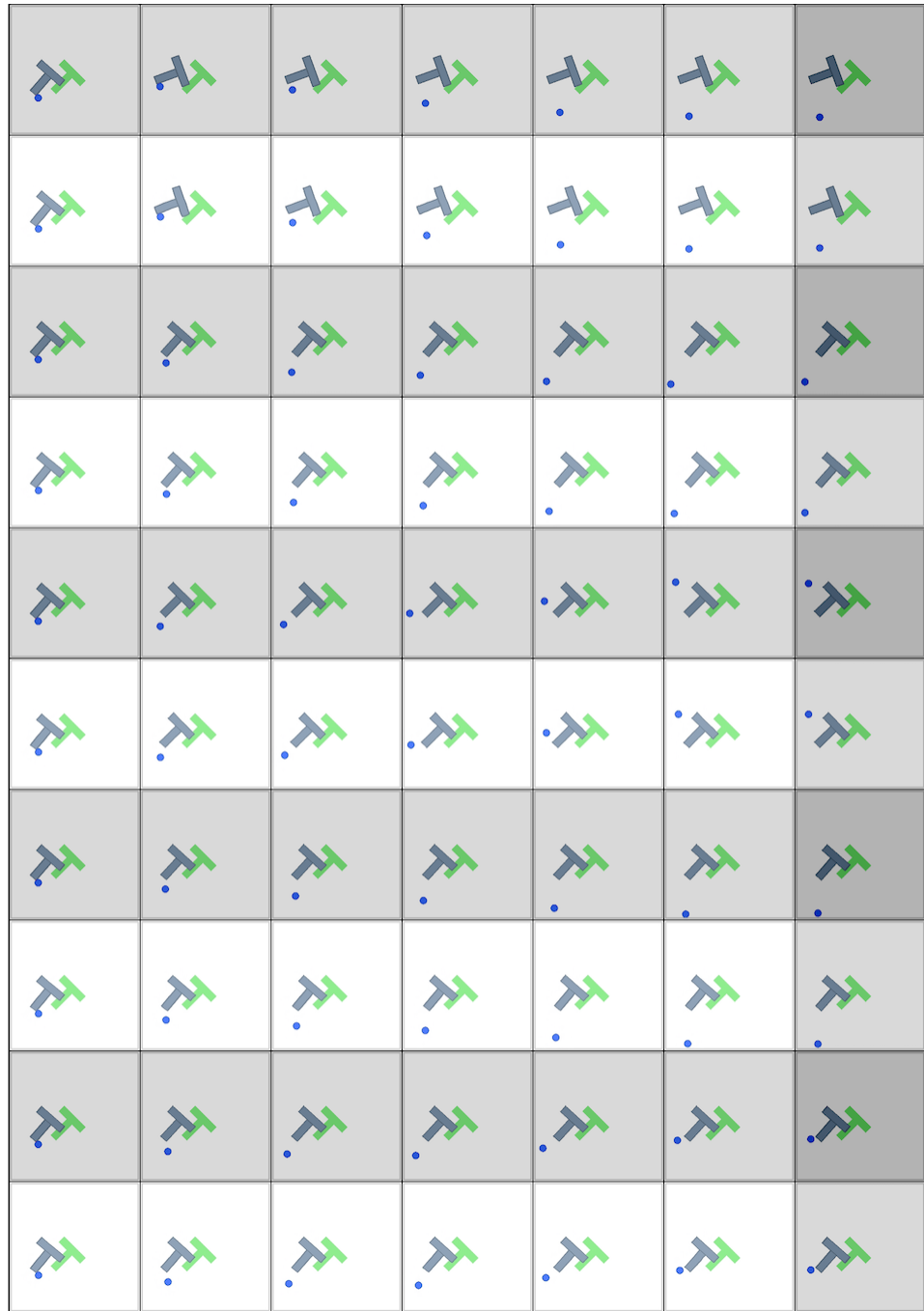


Figure 9: Trajectories planned with DINO-WM on PushT with the same initial states but different goal states.

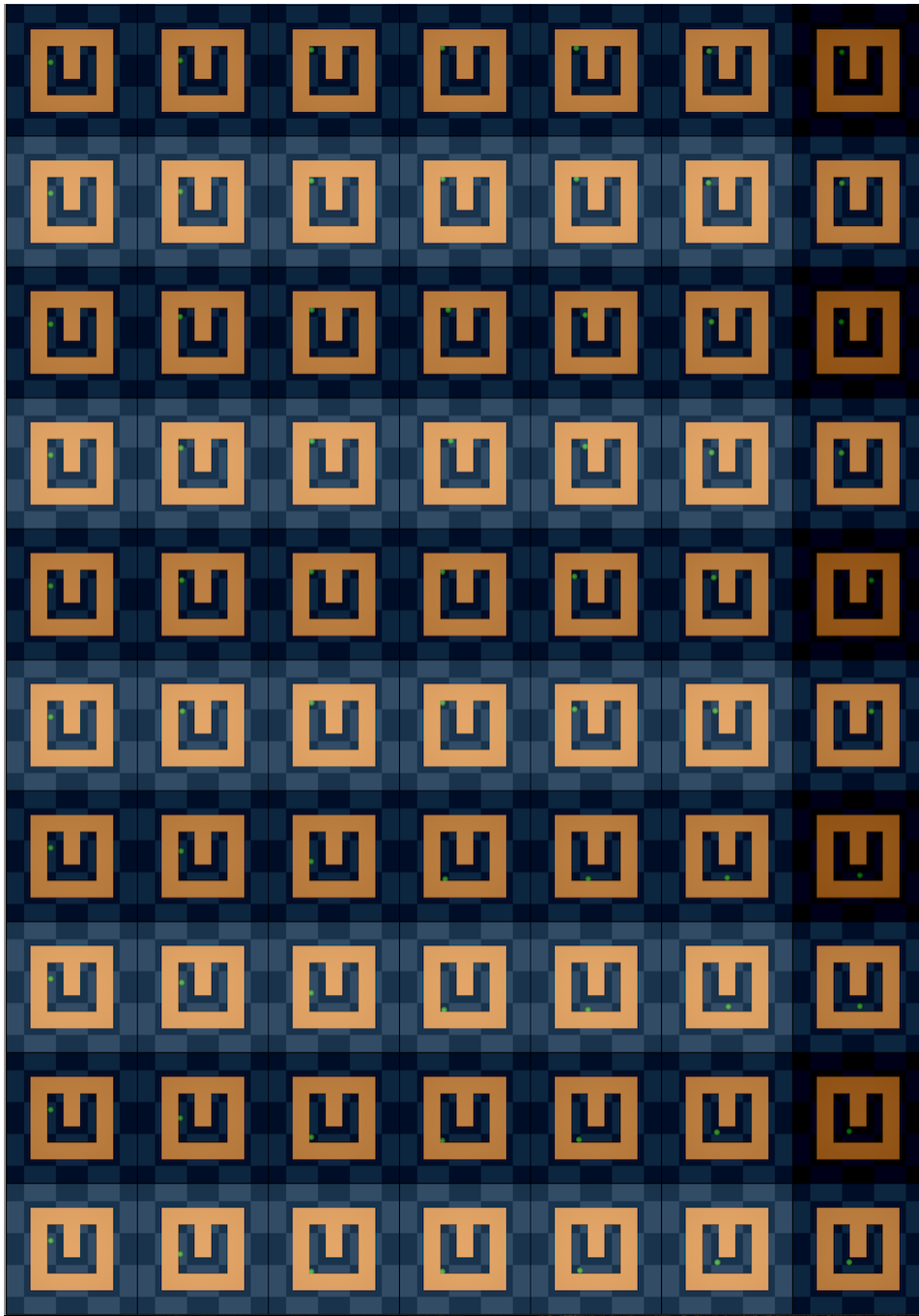


Figure 10: Trajectories planned with DINO-WM on PointMaze with the same initial states but different goal states.